Optical Model Analysis of ^{8}B+^{27}Al Elastic Scattering Above the Coulomb Barrier

S. R. Mokhtar[1], R. A. Abdel-Gahni[2,], M. Tammam[2] and M. El-Azab Farid [1]*

[1] Physics Department, Assiut University, Assiut 71516, Egypt.
[2] Physics Department, Al-Azhar University, Assiut 71524, Egypt.

Abstract: The angular distribution of ^{8}B elastic scattering cross section on ^{27}Al is studied at two energies above the Coulomb barrier, namely15.3 and 21.7 MeV. The analysis is performed in the framework of optical model (OM) potential. Semi-phenomenological and microscopic OM potentials are used. The sensitivity of our results to density distribution shape of ^{8}B nucleus is presented. Good agreement with the experimental data is obtained without renormalization factors. The calculated total reaction cross section is presented and compared with previous analysis.

Keywords: Optical potential, Double folding, Elastic scattering, Nuclear reactions, Halo nuclei.

1 Introduction

The so-called halo nuclei attracted a great attention in last decades [1-9]. These nuclei are located near the driplines and have interesting properties. Particular attention has been given to some of these nuclei such as ^{6}He and ^{8}B because of their exotic structure and it easy to get them as low-energy radioactive beams [10-15]**.** ^{8}B has a very low proton separation energy (0.138 MeV), hence it has more probability to ^{8}B→^{7}Be+p breakup. So, ^{8}B have been considered a p-halo nucleus [16-18].

Because of ^{8}B has very interesting properties and it has applications in important fields such as astrophysics [19], there are many experimental and theoretical works in the literature which interested in determining the unusual properties and the relation between different reaction channels in case of ^{8}B . Experimentally, the halo formation is confirmed for ^{8}B using some measurements such as, elastic scattering, quasi-elastic scattering, breakup reactions as well as the total reaction cross section [20-25].

Among the most striking experimental observations had appeared which clearly supported the existence of a neutron halo in the nucleus is the momentum distribution measurements. For ^{8}B it has been found that ^{7}Be has a narrow momentum distribution in breakup reactions of ^{8}B on C, Al, and Pb targets [21]. As well as, the measurement of interaction cross sections proved that ^{8}B has a large root-mean-square radius (rms) compared with heavier boron isotopes [26,27]. Using the relativistic mean-field (RMF)

calculations J. S. Wang et. al. compared between the proton and neutron radius of ^{8}B. They found that ^{8}B has proton matter radius larger than that of the neutron matter radius[28].

The elastic scattering differential cross section is commonly used as a proof of existence of halo in ^{8}B [11,29,30]. In [11], the authors introduce an evidence for existence of proton halo in ^{8}B depending on the large value of the reaction cross section. Experimental measurements and theoretical calculations have been performed to elastic scattering of ^{8}B, ^{7}Be, and ^{6}Li on a ^{12}C as a target [29]. The deduced total reaction cross sections were compared with that of weakly and tightly bound nuclei elastically scattered on ^{12}C as a function of energy. They found that, at energies around coulomb barrier the reduced total reaction cross sections are larger for ^{6}He and ^{8}B than that of the weakly bound nuclei, and the last is larger than that of the tightly bound nuclei. However, when the date is taken from high-energy experiments, there is difficulty to get evidence about the halo formation in the projectile, this attributed to that the halo is a surface phenomenon [29]. On the other hand, the breakup effects found to be negligible in case of some targets such as ^{12}C [30].

In the present study, the differential cross sections of proton halo nucleus ^{8}B elastically scattered on ^{27}Al at two incident energies above the coulomb barrier is calculated in the framework of OM potential. Four different shapes of ^{8}B density distribution is considered. This paper is organized as following. Sec. 2 contains the description of the OM potential that we used, while the results are presented in Sec.

*Corresponding author e-mail: rar.zidan@azhar.edu.eg

3. Finally, our main conclusions are presented in Sec. 4.

The previous discussion shows that the breakup reactions has a large effect in case of systems involving the very loosely bound ^{8}B. The most common method that used to study the effect of the breakup is the continuum discretized coupled-channels (CDCC) method [29-34]. Lubian et al. [32] studded the breakup channel effects on elastic scattering of ^{8}B + ^{58}Ni. They found that the experimental data is produced well when the continuum-continuum couplings are included. As well, Lubian et al. [35] carried out CDCC calculations to study effect of the breakup on the fusion and quasi-elastic barrier distributions for the same system. They found that the coupling with the breakup channel leads to the barrier distribution occur at higher energies. Recently the same proton-halo nuclei, is theoretically studied using CDCC method but with heavier nucleus ^{208}Pb as target [36]. They found that the elastic scattering can well reproduced by considering only the nuclear breakup.

On other hand the optical model potential (OM) method is the traditional method to studying the elastic-scattering differential cross sections and total reaction cross sections theoretically. It has two main categories, Woods-Saxon (WS) and double-folding (DF) potentials. Lukyanov et. al. studied the structure of ^{8}B using OM potential calculations. They instructed DF potential to calculate the elastic scattering cross section of ^{8}B on ^{12}C, ^{58}Ni, and ^{208}Pb targets. The real part includes direct and exchange terms, on other hand the imaginary part depending upon high-energy approximation (HEA) method. They concluded that, their microscopic DF potential can used well in analyzing reactions of systems include very exotic nuclei such as halo nuclei ^{8}B.

Most recent, Morcelle et. al. measured elastic scattering angular distributions for the system ^{8}B+^{27}Al at energies above Coulomb barrier, 15.3 and 21.7 MeV [9]. They performed WS potential and CDCC calculations to extract the angular distribution and reaction cross section. In CDCC calculations they used the global double folding São Paulo potential (SPP) [37]. Good agreement was achieved by two methods and the comparison between the elastic scattering with and without considering the breakup channels shows that these couplings reduce the Fresnel peak at backward angles and increase the reaction cross section.

2 Analysis of ^{8}B+^{27}Al elastic scattering

2.1 Optical model potential

In OM potential, the nuclear interaction between the two interacting nuclei is represented as potential with real V(R) and imaginary W(R) parts according to the relation:

$$V_N(R) = V(R) + iW(R), \qquad (1)$$

where R is the vector that separate between the projectile and the target centers of mass. In this case, the total OM potential is:

$$U(R) = V_N(R) + V_C(R), \qquad (2)$$

where $V_C(R)$ is a repulsive Coulomb potential, it is assumed to has double-sharp cutoff Coulomb potential shape [38], where,

$$V_C(R) = \begin{cases} \dfrac{z_P z_T e^2}{R}, & R > R_c, \\ \dfrac{z_P z_T e^2}{2R_c}\left[3 - \left(\dfrac{R}{R_c}\right)^2\right], & R \leq R_c, \end{cases} \qquad (3)$$

where $R_c = 1.3(A_P + A_T)^{1/3}$ is the radius of sphere has a uniform charge, A_P and A_T are the projectile and target mass numbers, respectively. In Eq. (3), Z_P and Z_T are the charge numbers of the projectile and target nuclei, respectively. In our work, we use the microscopic approach of the OM potential, where both real part is calculated microscopely by DF potential according to the following equation:

$$V_{DF}(R) = \int \rho_P(r_1)\rho_T(r_2)v_{nn}(s)\,d\vec{r_1}d\vec{r_2},$$
$$s = \left|\vec{R} - \vec{r_1} + \vec{r}\right| \qquad (4)$$

where ρ_P and ρ_T are the projectile (^{8}B) and the target (^{27}Al) ground-state density distributions, respectively, $v_{nn}(\vec{s})$ is the effective nucleon-nucleon (NN) interaction. Here, we take the NN interaction to be energy- and density-dependent form of M3Y effective interaction (DDM3Y), where,

$$v_{nn}(E, \rho, s) = g(E, s)f(E, \rho), \qquad (5)$$

where the original M3Y NN interaction $g(E, s)$ [39,40] is multiplied by a density-dependent factor $f(E, \rho)$ where,
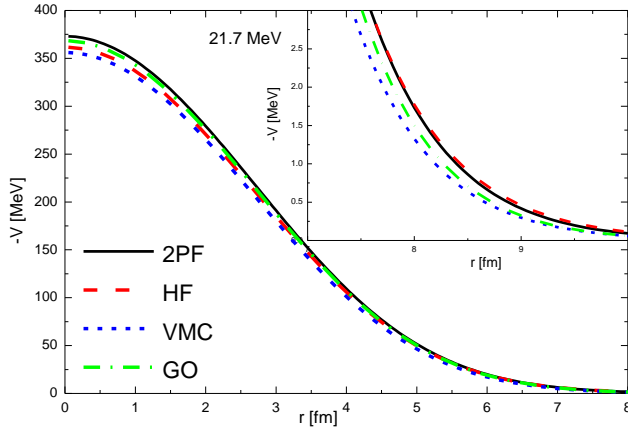
Figure 1. The real part of the OP model at 21.7 MeV calculated using 2PF, HF, VMC and GO density distributions. The inset graves focus on a specific region.
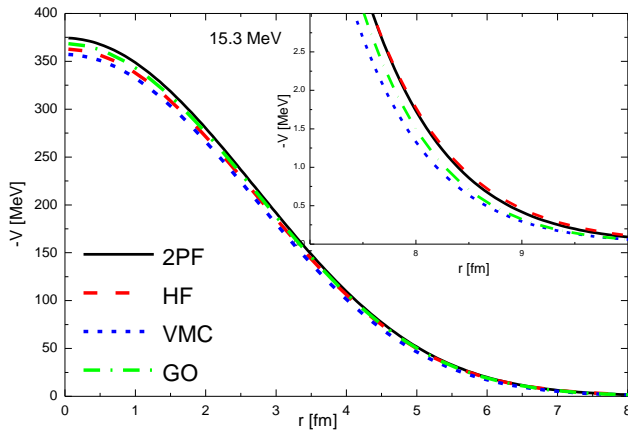
Figure 2. Same as Fig. 3 but at 15.3 MeV.

$$g(E,s) = \left(7999\frac{r^{-4s}}{4s} - 2134\frac{r^{-2.5s}}{2.5s}\right) + J_{00}(E)\delta(s), \tag{6}$$

where $J_{00}(E)\delta(s)$ simulate the knock-on exchange effects between the nucleons in the zero-range pseudo-potential, this term is weakly dependent on the incident energy as shown:

$$\hat{J}_{00}(E) = -276(1 - .005E)(MeV\ fm^3). \tag{7}$$

And:

$$f(E,\rho) = C(E)\left[1 + \alpha(E)e^{-\beta(E)\rho}\right], \tag{8}$$

where α, C and β are energy-dependent parameters, their values are taken from [40], E is the incident projectile energy per nucleon it has unit in MeV/nucleon. and $\rho = \rho_1\left(r_1 + \frac{1}{2}s\right) + \rho_2\left(r_2 + \frac{1}{2}s\right)$ is the nuclear matter density of colliding nuclei.

As a first step, the imaginary part of the optical potential is treated phenomenologically by considering the Woods-Saxon form factor $f(R)$:

$$W(R) = W_0 f(R), \tag{9}$$

Where W_0 is the imaginary potential depth and

$$f(R) = \frac{1}{1+\exp(\frac{R-R_x}{a})}, \tag{10}$$

where a is the diffuseness and the radius R_x can determine using the relation $R_x = r_0(A_P^{1/3} + A_T^{1/3})$, where $r_0 = 1.3\ fm$ is the reduced radii. Thus, the total OM potential (2) takes the form

$$U_A(R) = N_R V_{DF}(R) + W_0 f(R) + V_c(R) \tag{11}$$

In some cases, the imaginary part be the DF potential also, hence the total OM potentials become

$$U(R) = (N_R + iN_I)V_{DF}(R) + V_c(R), \tag{12}$$

where N_R and N_I are the real and imaginary renormalization factors.

2.2 Matter Density Distributions

In DF potential, the density distribution of colliding nuclei is very significant, where it has information about the structure of these nuclei. The OM analysis in this work consider various shapes of the projectile density distribution. For the target (^{27}Al) density distribution, we consider it has 2PF shape [41]:

$$\rho_{2PF}(r) = \frac{\rho_0}{1 + \exp\left(\frac{r-R}{a}\right)}, \tag{13}$$

where the radius R and the diffuseness a are equal 3.07 (fm) and 0.519 (fm), respectively. The parameter ρ_0 can be

produced from the normalization condition $4\pi \int \rho(r)r^2 dr = A$, where A is the mass number. This density form gives a root mean square (rms) radius of ^{27}Al equal 3.0621 fm. For the projectile (^{8}B) density distribution, we use three different shapes which consider various models of the internal nuclear structure, these densities are discussed in the following sub sections:

2.2.1 2PF density distribution.

The phenomenological 2PF, Eq. (13), is adopted to describe ^{8}B density distribution. In this case values of the radius and the diffuseness are R=1.8509 fm and a=0.5352 fm, respectively [42]. This density produces rms radius of ^{8}B equal 2.774 fm. In spite of that, the proton halo formation in case of ^{8}B is still open issue [43,44].
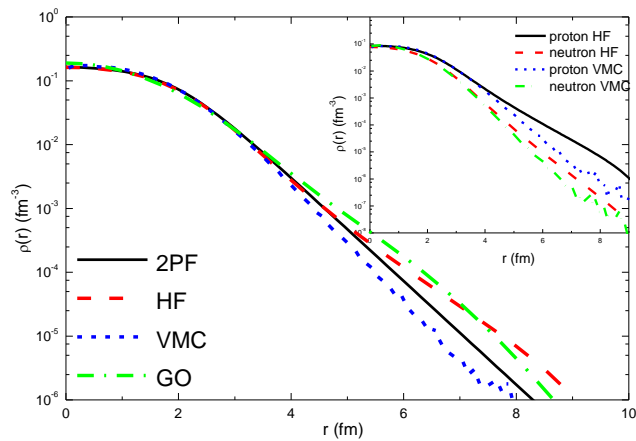


Figure 3. The density distributions for ^{8}B given all considered densities. The inset graphs show Point-proton and point-neutron density distribution calculated using HF and VMC.

2.2.2 The Variational Monte Carlo (VMC) density distribution.

The proton and neutron densities of ^{8}B nucleus have been obtained in a microscopic way by the Variational Monte Carlo (VMC) method [45,46]. The VMC method uses a realistic Hamiltonian containing the Argonne v18 (AV18) two-nucleon potential and Urbana X three-nucleon potentials (AV18+UX) to establish the variational wave function. For the sake of comparison, we use ^{8}B density that obtained form Hartree-Fock (HF) calculations [30]

2.2.3 The Gaussian-Oscillator (GO) density distribution
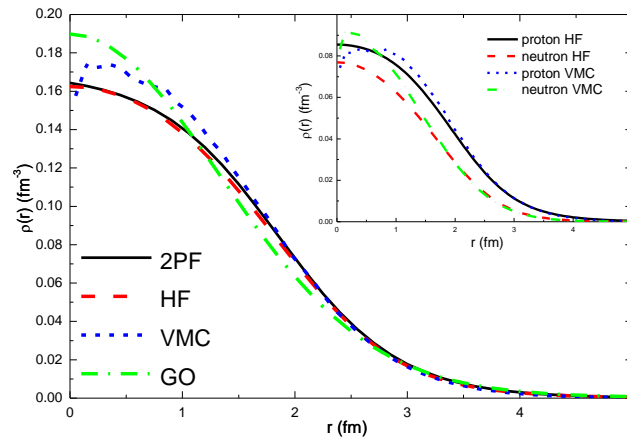
Figure 4. Same as Fig. 1, but in linear scale.

The core (^{7}Be) and halo (p) in ^{8}B nucleus are presented with different spatial distributions in some phenomenological density forms. The Gaussian-Oscillator (GO) density distribution considers the core has Gaussian density form:

$$\rho_c(r) = \left(\frac{3}{2\pi R_c^2}\right)^{3/2} \exp(-\frac{3r^2}{2R_c^2}), \qquad (14)$$

where R_c the rms radii of the core. On other hand, the halo density is taken to be 1p-shell harmonic oscillator density:

$$\rho_h(r) = \frac{5}{3}\left(\frac{5}{2\pi R_h^2}\right)^{3/2}\left(\frac{r}{R_h}\right)^2 \exp(-\frac{5r^2}{2R_h^2}), \qquad (15)$$

where R_h the rms radii of the halo. Both R_c and R_h radii are related to the matter radius of the projectile R_m as:

$$R_m = \left(\frac{N_c R_c^2 + N_h R_h^2}{A_m}\right) \qquad (16)$$

where N_c , N_h and A_m are numbers of nucleons in the core, halo and the projectile, respectively. Hence, the total matter distribution of ^{8}B is given by:

$$\rho_m(r) = N_c \rho_c(r) + N_h \rho_h(r) \qquad (17)$$

The values of is taken from [47], R_c , R_m equal 2.3 and 2.59 fm, respectively, and this density produces $R_h =$ 4.06 fm.

3 Results and discussions

A comparison between the density shapes of ^{8}B are shown in Fig. **3** in logarithmic scale, and in Fig. **4** in linear scale. One can observe that, the halo nature of ^{8}B are represents by extended tail in case of all considered densities. On other hand, in the center, GO density has a larger value, while VMC density has smallest radial extension. Both 2PF and HF densities have quite similar behavior in the region r $\approx$ 0-5 fm. Also, there is deference between all of them in the outer region. The proton halo nature of ^{8}B appear clearly in the inset graphs where the tail of the point-proton distribution is obviously greater than that of point-neutron distribution. These densities are considered when we study the OP analysis, the results are presented in the following discussion.

Table 1. The best fit W_0 values that produce best agreement with the experimental data for all considered densities. The energy (in MeV), reaction cross section in (mb) and chi square per nucleon are also listed.

E	Density	W_0	χ^2/N	σ_R
	2PF	59.40	0.519	1232
21.7	HF	58.13	0.528	1233
	VMC	61.21	0.505	1223
	GO	56.72	0.547	1241
	2PF	25.42	0.787	477
15.3	HF	23.79	0.799	476
	VMC	29.76	0.806	474
	GO	20.61	0.816	482

The DF potentials of ^{8}B+^{27}Al elastic scattering at incident energy 21.7 MeV are shown in Fig. **1** and that of incident energy 15.3 MeV are shown in Fig. **2**. The inset figures show behavior of the potentials on the surface region. It is quite noticeable that, the four density shapes produce potentials almost have the same behavior. The difference in the potentials derived using all densities slightly show up at the interior region, the potential of 2PF has deeper depth than the potentials of the other density distributions. For the sake of comparison, we insert the DF potential at energies 21.7 and 15.3 MeV. By comparison between Fig. **1** and Fig. **2** one can observe the reaction under study is weak energy dependence. That is not a general observation because of the narrow rage of the incident energy that considered. We can conclude that, the OP of the system ^{8}B+^{27}Al is low sensitive to the choice of ^{8}B density distribution. On the other hand, obviously, the derived potentials shown in Fig. **1** and Fig. **2** reflect the behavior of the corresponding density distributions shown in Fig. **3** and fig. **4**.

Table 2. The calculated total reaction cross section in (mb) and chi square per nucleon are produced by U_B for all density distributions.

| E	Density	χ^2/N	σ_R
	2PF	1.287	1024
21.7	HF	1.163	1059
	VMC	1.102	1034
	GO	0.963	1033
	2PF	0.837	448
15.3	HF	2.725	481
	VMC	1.278	374
	GO	0.870	499

In the framework of OP model, the elastic scattering differential cross section of the system ^{8}B+^{27}Al is calculated using DF potential based upon the density dependent version of M3Y (DDM3Y) and the 2PF, HF, VMC and GO density distribution. In our analysis we use two various models of OM potential, semi-phenomenological and microscopic OM, that we called them U_A and U_B, respectively. In the semi-phenomenological approach, the real part is calculated microscopely using, while, the imaginary part is calculate phenomenologically using as shown in Eq. (11). In the microscopic approach, the optical potential is a complex potential where the real and imaginary parts have the same shape Eq. (12).

Fitting data procedure: the starting point in our calculations is the WS parameters listed in [9]. Then the real WS part is replaced by the folding one. We found that, good fitting with the experimental data can obtained by considering the imaginary depth W_0 as a free parameter while the geometry parameters are fixed at $R_x = 1.3$ fm and a=0.65 fm. In a second step the imaginary WS part is replaced also by DF potential, in this case the free parameters are N_R and N_I, for the system under study, we found that the experimental data well produced by considering $N_R = N_I = 1$. All calculations in this study are performed using FRESCO code [48], while the fitting procedure is performed using the subroutine SFRESCO.

The results of U_A are shown in Fig. **5** and Fig. **6** for incident energies 21.7 and 15.3 MeV, respectively. And the results of U_B are shown in Fig. **7** and Fig. **8**, for incident energies 21.7 and 15.3 MeV, respectively. The best fit values for W_0, energy cross section and χ^2/N are shown in Table **1**. It is clearly observed that, U_A gives good fitting for all densities at both incident energies and this is reflected on the chi square values shown in Table **1**. There is no need to renormalize the real part to get the experimental data. Comparison between our results and the results of the same system analyzed using full phenomenological potential [9] shows that, at 21.7 MeV the calculated reaction cross section using semi-phenomenological potential is larger
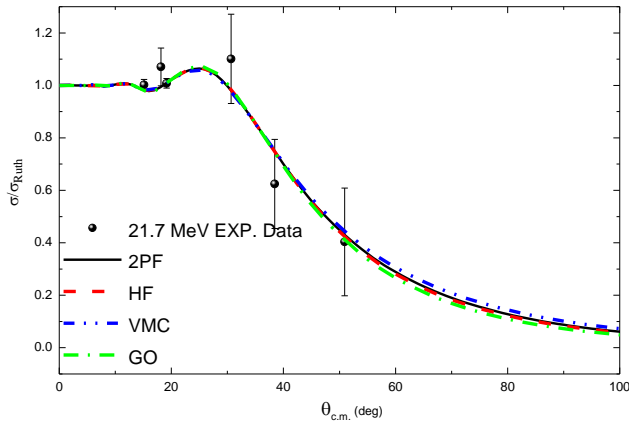
Figure 5. Angular distribution of the ^{8}B+^{27}Al elastic scattering differential cross section at 21.7 MeV and calculated using U$_A$ for all considered density distributions. The circles are the experimental data from [9].
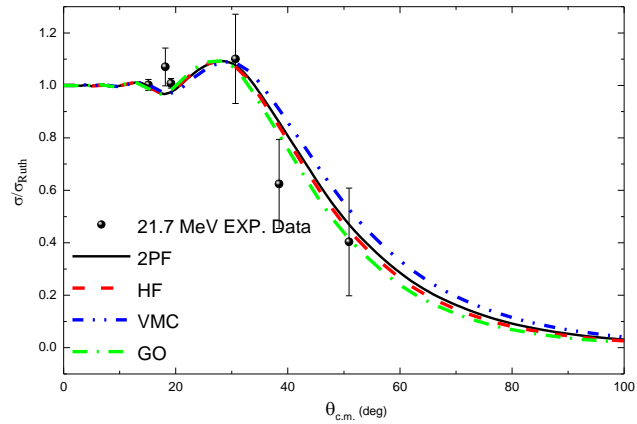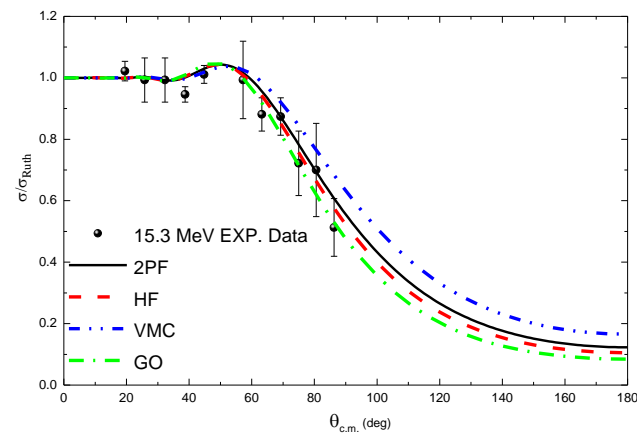

Figure 7. Same as Fig 5 but using U$_B$.
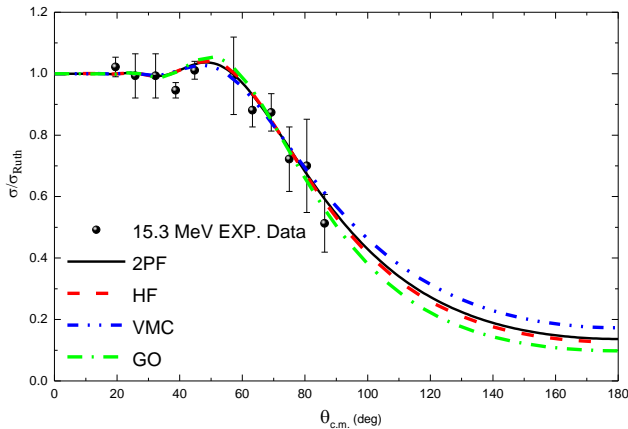
Figure 6. Same as Fig 5 but at incident energy 15.3 MeV

Figure 8. Same as Fig. 7 but at the incident energy 15.3 MeV

than that calculated using full phenomenological potential and vice versa for 15.4 MeV, this observation is achieved for density distributions. The values listed in Table **1** show that, at both energies, the GO density has lower imaginary depth while the CMV density has higher one. As shown in Fig. **5** and Fig. **6**, the deference between the curves is located at backward angles and growth up at the region that don't contain experimental data, this difference increases with the energy. The same behavior is observed in case of U$_B$ as shown in Figs. **7** and **8**.

On other hand, the results U$_B$ are shown in Table **2** and the corresponding elastic scattering differential cross sections are shown in Fig. **7** for incident energy 21.7 MeV and Fig. **8** for incident energy 15.3 MeV. One can see that; a quite good fitting is archived for all considered densities without any renormalization parameters ($N_R = N_I = 1$).

The GO density gives better fitting to the experimental data both two energies. The values in Table **1** and Table **2** and all results which we obtained show that 2PF and HF densities have the same behavior. However, the sensitivity of the results to the choice of the ^{8}B density distribution decreases with increases the incident energy.

4 Conclusions

In the present work, we use two different types of OM potential to calculates the elastic scattering differential cross section of the system ^{8}B+^{27}Al at incident energies 21.7 and 15.3 MeV. the first one is semi-phenomenological potential (U$_A$) and the second is microscopic potential (U$_B$). The microscopic potential is folded with four different density distributions, 2PF, HF, VMC and GO density distributions. The DDM3Y NN interaction is used in the folding process. With only one adjustable parameter in U$_A$ and without any adjustable parameters in U$_B$, good fitting with the experimental data is obtained. We found that the dependence of the angular distribution on ^{8}B density shape

decrease when the incident energy increases. On other hand the total reaction cross section increases with the increase of the incident energy. At E=21.7 MeV and for U_A, all densities produce total reaction cross section larger than that have been calculated using full phenomenological potential, while, vice versa for U_B.

Acknowledgement

References

[1] R. Lichtenhaler, A. Lepine-Szily, V. & Perego, C. & Camargo Jr., O. & Denke, R. & de Faria, PN & Benjamim, EA & Added, N. & Lima, GF & Hussein, MS & Kolata, J. & Arazai, A., Eur. Phys. J. A 25 (2005) 733.

[2] N. Keeley, R. Raabe, N. Alamanos, J. Sida, Progress in Particle and Nuclear Physics 59 (2007) 579.

[3] N. Keeley, N. Alamanos, K. Kemper, K. Rusek, Progress in Particle and Nuclear Physics 63 (2009) 396.

[4] B. Back, H. Esbensen, C. Jiang, K. Rehm, Reviews of Modern Physics 86 (2014) 317.

[5] A. Lépine-Szily, R. Lichtenthäler, V. Guimarães, The European Physical Journal A 50 (2014) 128.

[6] L. Canto, P. Gomes, R. Donangelo, J. Lubian, M. Hussein, Physics Reports 596 (2015) 1.

[7] P. Gomes, J. Lubian, L. Canto, D. Otomar, D.M. Junior, P. de Faria, R. Linares, L. Sigaud, J. Rangel, J. Ferreira, Few-Body Systems 57 (2016) 165.

[8] J. Kolata, V. Guimarães, E. Aguilera, The European Physical Journal A 52 (2016) 1.

[9] V. Morcelle, R. Lichtenthäler, A. Lépine-Szily, V. Guimarães, K. Pires, J. Lubian, D.M. Junior, P. de Faria, J. Kolata, F. Becchetti, Physical Review C 95 (2017) 014615.

[10] E. Aguilera, J. Kolata, F. Becchetti, P. DeYoung, J. Hinnefeld, Á. Horváth, L. Lamm, H.-Y. Lee, D. Lizcano, E. Martinez-Quiroz, Physical Review C 63 (2001) 061603.

[11] E. Aguilera, E. Martinez-Quiroz, D. Lizcano, A. Gómez-Camacho, J. Kolata, L. Lamm, V. Guimaraes, R. Lichtenthäler, O. Camargo, F. Becchetti, Physical Review C 79 (2009) 021601.

[12] E. Benjamim, A. Lépine-Szily, D.M. Junior, R. Lichtenthäler, V. Guimaraes, P. Gomes, L. Chamon, M. Hussein, A. Moro, A. Arazi, Physics Letters B 647 (2007) 30.

[13] P. De Faria, R. Lichtenthäler, K.C.C. Pires, A. Moro, A. Lépine-Szily, V. Guimaraes, D. Mendes Jr, A. Arazi, M. Rodríguez-Gallardo, A. Barioni, Physical Review C 81 (2010) 044605.

[14] L. Gasques, L. Chamon, D. Pereira, V. Guimaraes, A. Lépine-Szily, M. Alvarez, E. Rossi Jr, C. Silva, B. Carlson, J. Kolata, Physical Review C 67 (2003) 024602.

[15] M. Rodríguez-Gallardo, J. Arias, J. Gómez-Camacho, R. Johnson, A. Moro, I. Thompson, J. Tostevin, Physical Review C 77 (2008) 064609.

[16] H. Kitagawa, H. Sagawa, Physics Letters B 299 (1993) 1.

[17] T. Minamisono, T. Ohtsubo, I. Minami, S. Fukuda, A. Kitagawa, M. Fukuda, K. Matsuta, Y. Nojiri, S. Takeda, H. Sagawa, Physical review letters 69 (1992) 2058.

[18] H. Nakada, T. Otsuka, Physical Review C 49 (1994) 886.

[19] E.G. Adelberger, A. García, R.H. Robertson, K. Snover, A. Balantekin, K. Heeger, M. Ramsey-Musolf, D. Bemmerer, A. Junghans, C. Bertulani, Reviews of Modern Physics 83 (2011) 195.

[20] I. Pecina, R. Anne, D. Bazin, C. Borcea, V. Borrel, F. Carstoiu, J. Corre, Z. Dlouhy, A. Fomitchev, D. Guillemaud-Mueller, Physical Review C 52 (1995) 191.

[21] W. Schwab, H. Geissel, H. Lenske, K.-H. Behr, A. Brünle, K. Burkard, H. Irnich, T. Kobayashi, G. Kraus, A. Magel, Zeitschrift für Physik A Hadrons and Nuclei 350 (1995) 283.

[22] R. Warner, J. Kelley, P. Zecher, F. Becchetti, J. Brown, C. Carpenter, A. Galonsky, J. Kruse, A. Muthukrishnan, A. Nadasen, Physical Review C 52 (1995) R1166.

[23] J. Kelley, S.M. Austin, A. Azhari, D. Bazin, J. Brown, H. Esbensen, M. Fauerbach, M. Hellström, S. Hirzebruch, R. Kryger, Physical review letters 77 (1996) 5020.

[24] F. Negoita, C. Borcea, F. Carstoiu, M. Lewitowicz, M. Saint-Laurent, R. Anne, D. Bazin, J. Corre, P. Roussel-Chomaz, V. Borrel, Physical Review C 54 (1996) 1787.

[25] M. Smedberg, T. Baumann, T. Aumann, L. Axelsson, U. Bergmann, M. Borge, D. Cortina-Gil, L. Fraile, H. Geissel, L. Grigorenko, Physics Letters B 452 (1999) 1.

[26] I. Tanihata, T. Kobayashi, O. Yamakawa, S. Shimoura, K. Ekuni, K. Sugimoto, N. Takahashi, T. Shimoda, H. Sato, Physics Letters B 206 (1988) 592.

[27] M. Obuti, T. Kobayashi, D. Hirata, Y. Ogawa, A. Ozawa, K. Sugimoto, I. Tanihata, D. Olson, W. Christie, H. Wieman, Nuclear Physics A 609 (1996) 74.

[28] J. Wang, W. Shen, Z. Zhu, J. Feng, Z. Guo, W. Zhan, G. Xiao, X. Cai, D. Fang, H. Zhang, Nuclear Physics A 691 (2001) 618.

[29] A. Barioni, J. Zamora, V. Guimaraes, B. Paes, J. Lubian, E. Aguilera, J. Kolata, A. Roberts, F. Becchetti, A. Villano, Physical Review C 84 (2011) 014603.

[30] Y. Yang, J. Wang, Q. Wang, D. Pang, J. Ma, M. Huang, J. Han, P. Ma, S. Jin, Z. Bai, Physical Review C 87 (2013) 044613.

[31] F. Nunes, I. Thompson, Physical Review C 57 (1998) R2818.

[32] J. Lubian, T. Correa, E. Aguilera, L. Canto, A. Gomez-Camacho, E. Quiroz, P. Gomes, Physical Review C 79 (2009) 064605.

[33] B. Paes, J. Lubian, P.R.S. Gomes, V. Guimaraes, Nuclear Physics A 890 (2012) 1.

[34] B. Mukeru, M.L. Lekala, A. Denikin, Nuclear Physics A 935 (2015) 18.

[35] J. Lubian, T. Correa, P. Gomes, L. Canto, Physical Review C 78 (2008) 064615.

[36] J. Rangel, J. Lubian, L. Canto, P. Gomes, Physical Review C 93 (2016) 054610.

[37] L.C. Chamon, B.V. Carlson, L.R. Gasques, D. Pereira, C. De Conti, M. Alvarez, M.S. Hussein, M.C. Ribeiro, E. Rossi Jr, C. Silva, Physical Review C 66 (2002) 014610.

[38] R. Devries, M. Clover, Nuclear Physics A 243 (1975) 528.

[39] G.R. Satchler, W.G. Love, Physics Reports 55 (1979) 183.

[40] M.E.-A. Farid, G. Satchler, Nuclear Physics A 438 (1985) 525.

[41] S. Seyyedi, H. Golnarkar, Chinese physics C 39 (2015) 084103.

[42] A.S. Al-Hajjaji, PhD thesis, , Faculty of Science, Assiut University, 2014.

[43] S. Mizutori, J. Dobaczewski, G. Lalazissis, W. Nazarewicz, P.-G. Reinhard, Physical Review C 61 (2000) 044326.

[44] Y. Suzuki, K. Yabana, R.G. Lovas, K. Varga, Structure and reactions of light exotic nuclei, CRC Press, 2003.

[45] J. Carlson, S. Gandolfi, F. Pederiva, S.C. Pieper, R. Schiavilla, K. Schmidt, R.B. Wiringa, Reviews of Modern Physics 87 (2015) 1067.

[46] S.C. Pieper. Personal communication.

[47] S. Ilieva, PhD thesis, Johannes Gutenberg-Universität in Mainz, 2008.

[48] I.J. Thompson, Computer Physics Reports 7 (1988) 167.